# Ambient Seismic Recordings and Distributed Acoustic Sensing (DAS): Imaging the firn layer on Rutford Ice Stream, Antarctica

Wen Zhou[1], Antony Butcher[1], Alex Mark Brisbourne[2], Sofia-Katerina Kufner[2], John-Michael Kendall[3], and Anna Stork[4]

[1]University of Bristol
[2]British Antarctic Survey
[3]University of Oxford
[4]Silixa

November 30, 2022



**Abstract**

Distributed acoustic sensing (DAS) is a rapidly growing seismic technology, which provides near-continuous spatial sampling, low maintenance, long-term deployments, can exploit extensive cable networks already deployed in many environments. Here, we present a case study from the Rutford Ice Stream, Antarctica, showing how the ice-sheet firn layer can be imaged with DAS and seismic interferometry, exploiting noise from a power generator and fracturing at the ice stream margin. Conventional cross-correlation interferometry between DAS channels yields an unstable seismic response. Instead, we present two strategies to improve interferograms: (1) combining signals from conventional seismic instruments with DAS; (2) selective-stacking cross-correlation. These steps yield high-quality Rayleigh wave responses. We validate our approach with a dataset acquired using a sledgehammer-and-plate source, and show an excellent agreement between the dispersion curves. The passive results display a lower frequency content (~3Hz) than the active datasets (~10Hz). A 1D S-wave velocity profile is inverted for the top 100m of the glacier, which contains inflections as predicted by firn densification models. Using a triangular DAS array, we repeat the noise interferometry analysis and find no visible effect of seismic anisotropy in the uppermost 80 meters of our study site. Results presented here highlight the potential of DAS and surface wave inversions to complement conventional refraction surveys, which are often used for imaging firn layer, and the potential in near-surface imaging applications in general.

# Ambient Seismic Recordings and Distributed Acoustic Sensing (DAS): Imaging the firn layer on Rutford Ice Stream, Antarctica

**Wen Zhou[1], Antony Butcher[1], Alex Brisbourne[2], Sofia-Katerina Kufner[2], J-Michael Kendall[3], Anna Stork[4]**

[1]University of Bristol, BS8 1TH, Bristol, UK

[2]British Antarctic Survey, CB3 0ET, Cambridge, UK

[3]University of Oxford, OX1 2JD, Oxford, UK

[4]Silixa, WD6 3SN, Borehamwood, UK

Corresponding author: Wen Zhou (wz18709@bristol.ac.uk)

**Key Points:**

- Improving DAS noise interferometry by hybrid instrumenting with a geophone or by selective stacking transient noise sources.
- A 1D S wave velocity profile for the firn layer (0 - 100 m), is inverted from the ambient seismic field.
- Using a triangular array, we observe the top 80 m of the firn layer to be seismic isotropic, at the study site.

## Abstract

Distributed acoustic sensing (DAS) is a rapidly growing seismic technology, which provides near-continuous spatial sampling, low maintenance, long-term deployments, can exploit extensive cable networks already deployed in many environments. Here, we present a case study from the Rutford Ice Stream, Antarctica, showing how the ice-sheet firn layer can be imaged with DAS and seismic interferometry, exploiting noise from a power generator and fracturing at the ice stream margin. Conventional cross-correlation interferometry between DAS channels yields an unstable seismic response. Instead, we present two strategies to improve interferograms: (1) hybrid instrumenting – combining conventional seismic instruments with DAS; (2) selective-stacking cross-correlation. These steps yield high-quality Rayleigh wave responses. We validate our approach with a dataset acquired using a sledgehammer-and-plate source, and show an excellent agreement between the dispersion curves. The passive results display a lower frequency content (~3Hz) than the active datasets (~10Hz). A 1D S-wave velocity profile is inverted for the top 100m of the glacier, which contains inflections as predicted by firn densification models. Using a triangular DAS array, we repeat the noise interferometry analysis and find no visible effect of seismic anisotropy in the uppermost 80 meters of our study site. Results presented here highlight the potential of DAS and surface wave inversions to complement conventional refraction surveys, which are often used for imaging firn layer, and the potential in near-surface imaging applications in general.



## Plain Language Summary

Using fibre optic cables as distributed acoustic sensing (DAS) to sense seismic waves is an emerging technology. It is particularly attractive to use ambient noise recorded by these cables to image shallow subsurface – for studying groundwater, pollution, ground stability, and seismic hazard, for examples. We develop a new approach for using DAS to image the near-surface, presenting results for the Rutford Ice Stream, Antarctica. Ice sheets and glaciers are often topped with a layer of snow that increases in density with depth until solid ice is reached. This is known as the firn layer, which contains air bubbles that hold insights into the paleoclimate, and crevasses that tell us about the stress field. We find seismic noise sources from a power generator and from distant crevassing to image the firn layer. We show how the use of a conventional seismic sensor (geophone) in conjunction with DAS improves imaging clarity. We also employ a selective approach in stacking the data. These results show good agreement with those obtained using a more conventional seismic source (a sledgehammer). This successful demonstration of firn layer imaging shows the potential for using DAS and ambient noise for near-surface imaging in general.


## 1 Introduction

Seismic monitoring provides an important and non-intrusive method of imaging the subsurface structure, especially given developments in Distributed Acoustic Sensing (DAS) and ambient noise interferometry. DAS is an optical fibre sensing technology that offers the potential of broadband frequency recording and near-continuous spatial sampling of earth strain and temperature variation signals (Ajo-Franklin et al., 2019; Ide et al., 2021). Taking advantage of spare fibres which are deployed for telecom usage (dark fibres), DAS data acquisition can be much easier and cheaper compared with conventional seismic instruments (Ajo-Franklin et al., 2019; Lindsey et al., 2020b; Rodríguez Tribaldos et al., 2019; Rodríguez Tribaldos & Ajo-

Franklin, 2021). In regions with no pre-installed optical fibre, deployment of fibre-optic cables is required. Nevertheless, DAS measurement is still very attractive as it provides unprecedented spatial coverage, which could improve the spatial resolution of subsurface images (Ajo-Franklin et al., 2019; Dou et al., 2017; Lellouch et al., 2019; Rodríguez Tribaldos et al., 2019; Rodríguez Tribaldos & Ajo-Franklin, 2021; Spica, Nishida, et al., 2020; Williams et al., 2019).

The sensing element of DAS is the optical fibre and so the sensor has no electronic or mechanical components, it therefore makes the technology an attractive option for long-term, low maintenance deployments in harsh environments (Lellouch et al., 2019; Mateeva et al., 2017; Spica, Nishida, et al., 2020). This makes it ideal for long term seismic monitoring in applications such as subsurface reservoirs (e.g., geothermal, hydrocarbon or hydrogen storage; Correa et al., 2018), submarine environments (Lior, Sladen, et al., 2021; Spica, Nishida, et al., 2020; Williams et al., 2019), critical infrastructure (e.g. nuclear plants; Butcher et al., 2021) and glacial studies (Booth et al., 2020; Brisbourne et al., 2021; Hudson, Kendall, et al., 2021; Walter et al., 2020).

When using surface waves, the depth of the measurement is directly related to the period of the signal, with higher frequencies confined to the shallow subsurface and lower frequencies extending to greater depths. Passive seismic methods provide advantages over active source methods due to their lower cost and deeper surface wave penetration (with lower surface wave frequency signal) and are potentially ideal for long-term seismic monitoring of subsurface. In recent years, we have seen successful applications of DAS for ambient surface wave imaging on submarine environments, using microseism noise 0.6 - 1 Hz (Spica, Nishida, et al., 2020), 0.5 - 5 Hz (Cheng et al., 2021) and 1 - 3 Hz (Lior, Mercerat, et al., 2021). The advantage of recording in the offshore environment is the stable seafloor temperature and shorter distance to microseism noise sources. Onshore applications have been also successful (e.g., Dou et al., 2017; Rodríguez Tribaldos & Ajo-Franklin, 2021; Spica, Perton, et al., 2020), with reported applications mostly limited to urban environments with strong anthropogenic (traffic, mechanical) noises at frequencies typically above 5 Hz. It is an open question, as to whether low-frequency seismic noise (below 1 Hz) is recorded with onshore DAS (with larger fluctuation in temperature and lower microseism signal level) and whether DAS can be employed for ambient surface wave imaging at remote areas with little or no anthropogenic noises.

The firn layer results from the densification and metamorphosis of snow into glacial ice. Through burial by subsequent accumulation, the overburden weight compacts the snow and reduces porosity by grain packing, deformation and sintering (Alley, 1987; Cuffey & Paterson, 2010). The depth-density profile is controlled primarily by the temperature and snow accumulation rate and is highly variable due to the broad range of climatic conditions across the continent (e.g., van den Broeke, 2008). Knowledge of the firn profile is critical for improving altimetric mass-balance estimates (Shepherd et al., 2012) and palaeo-climate reconstructions using ice cores (Craig et al., 1988). Additionally, studying firn layer properties may help better constrain models of surface melt leading to ice shelf retreat (van den Broeke, 2005). More recently, the study by Riverman et al. (2019) found that firn densification could be accelerated by shear stress along shear margins of ice streams.

A specific application of seismic refraction was developed for the investigation of firn by Kirchner & Bentley (1979). The method uses curve fitting with a double-exponential form applied to diving wave travel times, prior to a Wiechert-Herglotz-Bateman (WHB) velocity-depth inversion (Slichter, 1932). This method is commonly used to correct seismic reflection surveys for near-surface effects (e.g., Smith, 1997), derive elastic properties of firn (King & Jarvis, 2007; Schlegel et al., 2019), and investigate spatial and azimuthal variations (Hollmann et al., 2021; Kirchner & Bentley, 1979, 2013; Riverman et al., 2019). Limitations of this method relate to the requirement for WHI of a smooth and continuously increasing velocity profile and also the assignment of a specific profile shape as a result of the double exponential travel time curve fitting step. Although the method is viable for both P- and S-wave velocity measurement, the former is by far the most widely studied due to the greater ease of generation and identification of P-wave energy.

Passive seismic data and ambient noise methods have also recently been used to constrain variation in the ice and firn. For example, Walter et al. (2015) used surface wave energy from crevasse events to derive Green's functions between stations (broadband seismometers). Sergeant et al. (2020) derived Green's functions between stations at a range of sites in Greenland and the Alps using a range of noise sources. Again, in an Alpine setting at Glacier de la Plaine Morte, Switzerland, measurements of azimuthal variation in Rayleigh wave velocity indicate that crevasses cause up to 8% anisotropy (Lindner et al., 2019).

In this manuscript, we investigate the feasibility of using DAS ambient noise analysis to image the firn layer. First, we show, based on data from a linear DAS cable, that DAS data can be used to derive a velocity profile with ambient noise interferometry (ANI) methods. As a verification, we compare these results against dispersion analysis of the surface waves captured by an active survey. Second, we use the data from a triangular array to investigate lateral heterogeneity and anisotropy of the firn. We demonstrate the viability and potential advantages of the method compared to the more widely used active source methods described above.

### 1.1 Field experiment at the Rutford Ice Stream and data acquisition

Between 11th and 24th January 2020, both active and passive seismic surveys were acquired over the Rutford Ice Stream (RIS), West Antarctica. The resulting dataset includes continuous data recorded on linear and triangular DAS fibre optic arrays and 3-component geophones (Figure 1). The purpose of this dataset is to investigate how well DAS data and processing methods can be used to record icequakes (microearthquakes that originate from the base of RIS) and to interrogate the internal properties of the ice column. RIS is particularly suitable for this study as icequakes are abundant, the seismic waveforms typically have high signal-to-noise ratios (SNR) and the velocity structure is relatively simple and well constrained.

RIS is a fast-flowing ice stream draining part of the West Antarctic Ice Sheet into the Ronne Ice Shelf. At the experiment site, RIS is around 25 km wide and 2200 m thick, flowing at 377 m a-1 (Murray et al., 2007). The seismic arrays are installed at the centre of the stream where the surface is relatively flat. Naturally occurring icequakes are a regular occurrence at the interface where the glacier slides over its bed (Kufner et al., 2021; Smith et al., 2015). Hudson et al. (2021) examined the suitability of DAS for passive seismic monitoring in this setting and detected fewer icequakes than with the standard geophone array. This was primarily due to the lower SNR of the DAS array, which can be partially overcome by array-based processing methods (Butcher, Hudson, et al., 2021). Using the source spectra of these icequakes, Hudson et al. (2021) observed signals below 1 Hz in the DAS dataset (with buried cable), which they suggest indicates it could be useful for ambient noise studies.

A seismic refraction profile was previously acquired 2.6 km upstream of the experiment site using a surface source and expanding spread of vertical component geophones out to a maximum offset of 980 m, as part of the site survey for the Beamish subglacial drilling project (Smith et al., 2021). A P-wave velocity depth profile was derived using the WHB based inversion method of Kirchner & Bentley (1979) (Figure 1c). With this method, Kirchner & Bentley (2013) report velocity uncertainty of ±60 m s-1 near the surface, reducing to ±30 m s-1 at 10 m depth and ±15 m s-1 at 50 m depth.

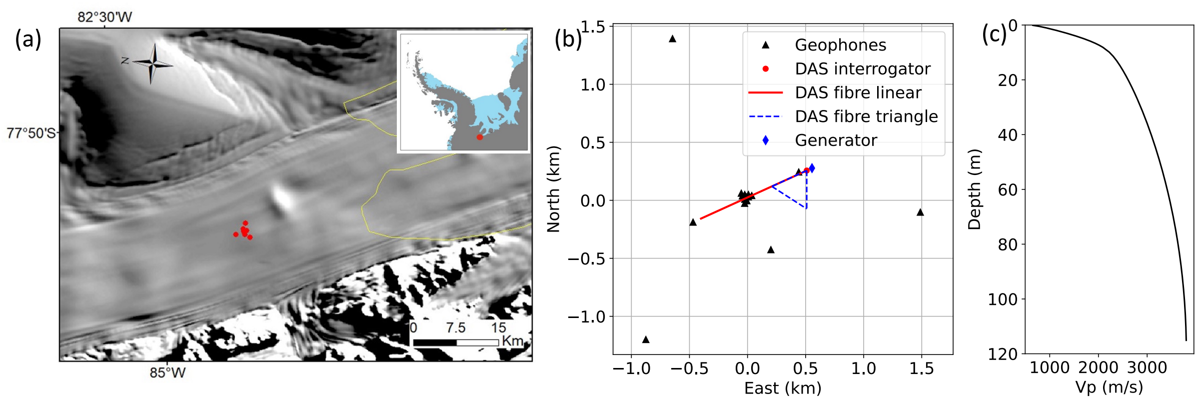


*Figure 1. (a) Location of seismic experiment on RIS. Geophone stations are shown as red dots. The background is Moderate-resolution Imaging Spectroradiometer (MODIS) imagery (Scambos et al., 2007). The MEaSUREs grounding line is in yellow (Rignot et al., 2011). (b) The relative position of geophones and DAS fibre. (c) Firn P wave velocity profile from previous refraction experiment (Smith et al., 2021), using an expanding interval vertical component geophone spread.*

DAS data were acquired using a Silixa iDAS v2 interrogator connected to a 1 km fibre optic cable deployed in linear and triangular configurations. Alongside the passive measurements, an active seismic survey was also acquired along the linear array using a hammer and plate source. Data were recorded using a 1 kHz and 8 kHz sampling rate for passive and active measurements respectively, with a 10 m gauge length and a 1 m channel spacing. A petrol generator was deployed as the power supply. The generator is located 50 m away from the interrogator (Figure 1b). Multiple shots were acquired at a 50 m spacing along the array using a hammer and plate. This generated shot gathers which display seismic signals spanning the majority of the linear array. An example shot gather from this survey is displayed in Figure 2, which shows clear surface wave dispersion. Due to timing difficulties, the shot times are poorly constrained.

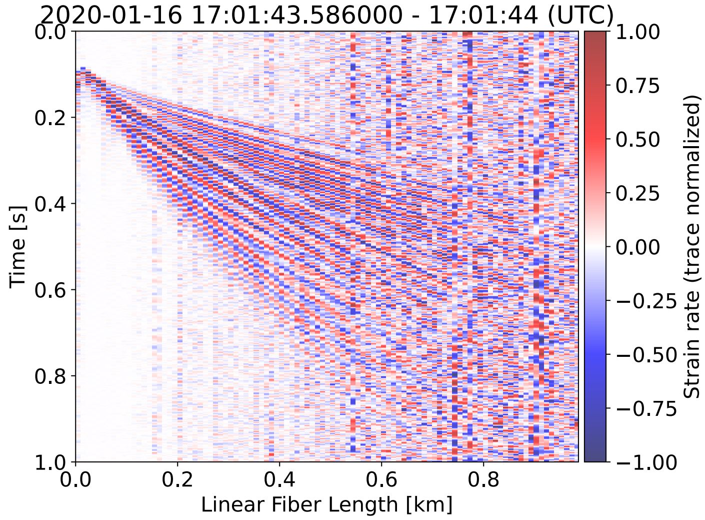


*Figure 2. Shot gather generated using a hammer and plate source, bandpass filtered 5 to 100 Hz. Body and surface waves are recorded across the majority of the linear array.*

DAS is a high-frequency strain sensing technique that contains one optical fibre as its sensing element and an interrogator as its data acquisition system. The basic principle of DAS is that backscattered laser signals are phase-shifted when the fibre experiences an extension or compression over a gauge length (He et al., 2017). Thus, DAS naturally measures compressional strain along the fibre; depending on the geometries of fibre and wave propagation, both P- and S-waves can be recorded.

The geophone network consisted of sixteen 4.5 Hz geophones with Reftek RT130 dataloggers with a 1 kHz sample rate. The geophone array layout was primarily optimised to detect and locate icequakes (Figure 1b). Three geophones were co-located or lie in-line with the fibre, which were approximately positioned in the middle and at either end of the linear DAS array.

In this manuscript, we investigate the feasibility of using DAS ambient noise analysis to image the firn at RIS. First, based on data from a linearly arranged DAS cable, we show that DAS data can be used to derive a velocity profile with ambient noise interferometry (ANI) methods. As a verification, we compare these results against dispersion analysis of the surface waves captured by the active survey. Second, we use the data from a triangular array to investigate lateral heterogeneity and anisotropy of the firn.

## 2 Ambient Noise Interferometry (ANI)

Since the first modern approaches by Shapiro et al. (2005) and Shapiro & Campillo (2004), ANI has become a well-established technique to obtain seismic velocity, especially surface wave velocities (Bensen et al., 2007), from ambient seismic noise. An extensive literature review of the subject is provided by Snieder & Larose (2013). By performing cross-correlation (CC) and stacking of recordings from receiver pairs, ANI derives an impulse response (Green's Function) between the receivers. Recent studies have implemented ANI with DAS data for borehole (Lellouch et al., 2019), submarine (Cheng et al., 2021; Spica, Perton, et al., 2020), and urban environment (Ajo-Franklin et al., 2019; Dou et al., 2017; Spica, Perton, et al., 2020). These studies generally take the same approach as when recordings of conventional seismometers or geophones are used. Another approach was taken by Spica, Nishida, et al.

(2020), who stack signals in the frequency-wavenumber (f-k) domain to direct retrieve surface wave dispersions. Since the performing of f-k transform is more expensive than cross-correlation in terms of computation time, we also take the conventional approach. However, in the supplementary material, a comparison between cross-correlation, deconvolution and f-k domain stacking is provided for measuring surface wave dispersions.

Spectrum whitened CCs are calculated using:

$$c_i(\omega) = \frac{1}{N}\sum_{t=0}^{N} \frac{r_i(\omega)s(\omega)^*}{\sqrt{\overline{r_i(\omega)^2}\;\overline{s(\omega)^2}}}, \qquad i = 1, 2, \dots m$$

where $s(\omega)$ is the reference channel, $r_i(\omega)$ represents one DAS channel ($m = 1250$ for the linear array). $N$ stands for the total number of windows stacked. After applying a tapered cosine window in the time domain, the power spectra, $r_i(\omega)^2$ and $s(\omega)^2$, are calculated and further smoothed by a 21-sample moving averaging. Time domain normalization was not applied, as testing indicated that the 1-bit normalization does not improve signal quality at this site. As the dominant seismic noises are above 1 Hz (see next section) we choose a window length of 10 seconds, with an overlap of 5 seconds and linearly stack over every 2 minutes, which results in $N = 23$. We do not attempt to remove the icequakes signals at this stage, as their magnitudes are generally small as reported by (Hudson, Baird, et al., 2021; Kufner et al., 2021) and are therefore of the same order of amplitude as the noise on the DAS channels (Hudson, Kendall, et al., 2021). As will be seen in the following section, these high frequency icequake signals are diminished when stacking CCs as they do not exhibit a stationary surface wave response. As ANI is a relatively new application to DAS data in a glacial setting (Walter et al., 2020), we first investigate the characteristics of the ambient noise before CC is performed.

## 2.1 Characteristics of ambient noise recorded on the RIS DAS array

Ahead of the creation of dispersion curves from the passive dataset, we seek to characterise some of the seismic noise sources recorded on the DAS array. In Figure 3 we present an example of high frequency noise, which begins abruptly and appears to originate close to one end of the array (0 m). We examine the frequency content of this signal by creating a spectrogram at 120m (Figure 3c) along the array using a short time Fourier transform (STFT). The signal starts with a gradually increasing amplitude over 10 to 80 Hz from around 25 s, then settles at a constant frequency around 40 Hz and 50 Hz at ~70 s. From 120 s, the signal frequency content and amplitude both increases until an abrupt stop at 145 s. From the pattern of this signal, we suspect it is likely noises from human activity at the interrogator site, most likely from a petrol generator that provides electricity supply (Figure 1b).

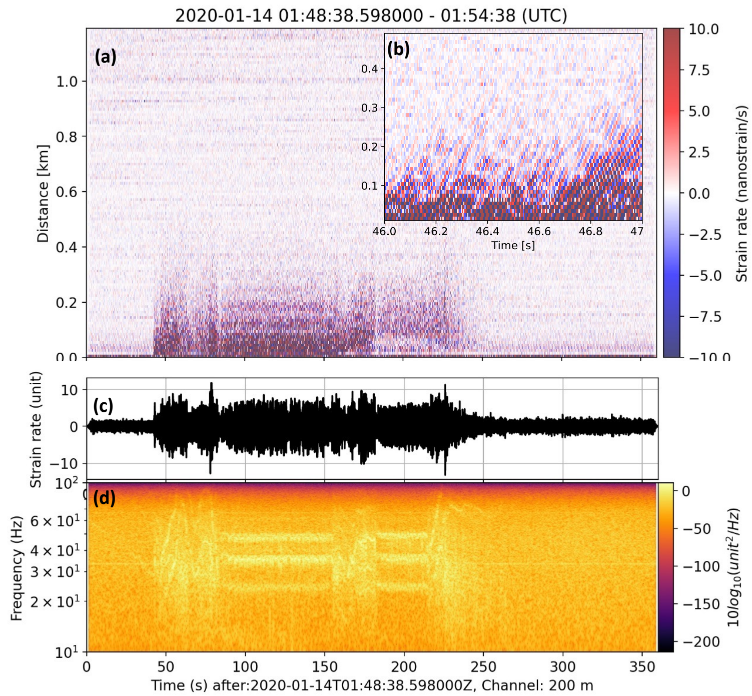


*Figure 3. (a) Six minutes of DAS recording after median value been subtracted for each time step, and bandpass filter 10 to 70 Hz. (b) A zoom-in of (a) for 46-47 seconds at 0 to 500 m. (c) Time series for DAS channel at 200 m. (d) Spectrogram for (c), with amplitude in log scale.*

An example of a low-frequency transient surface wave event is shown in Figure 4. The exact origin time and location of this event are not determined with the linear fibre, but we can expect it is travelling from northeast to southwest, nearly parallel to the fibre, because its apparent velocity (around 1800 m/s) is close to surface wave velocity below 10 Hz (Figure 9). The dispersion feature of the signal is clearly shown in the spectrogram in Figure 4c. More than 2000 of such events are detected using the geophone array, and using traveltime differences among the geophone array, 248 of such events are located and reported in the supplementary information (Figure S4). They appear to originate from the shear margin of the glacier. The exact sources of these signals are not resolved in the study, but crevasses and ice fracture at and beyond the shear margins are two potential candidates. Similar signals are thought to have contributed to ambient noise analysis at an Alpine glacier (Walter et al., 2015, 2020).

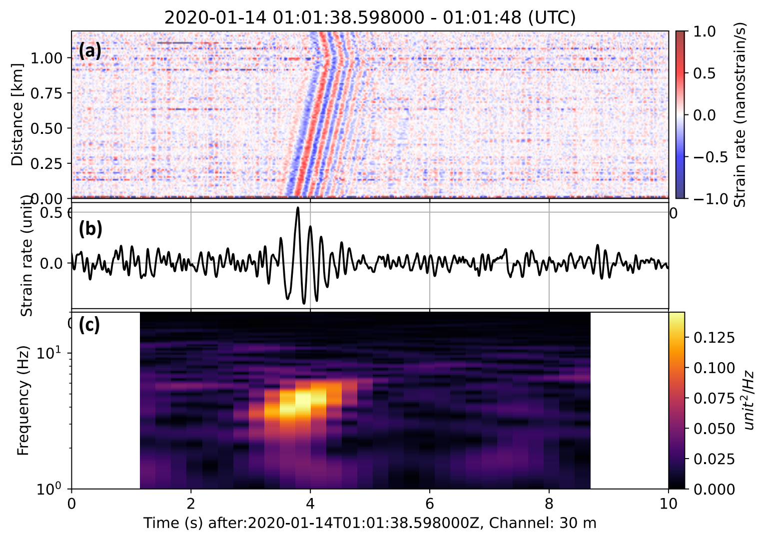


*Figure 4. (a) Ten seconds of DAS strain rate measurement after median removal and bandpass filter 1 to 10 Hz. (b) Waveform plot for the channel at 30 m offset. (c)Spectrogram of (b).*

Coherent signals are observed at periods beyond 100 seconds (Figure 5a). These signals are mostly travelling from far offset towards near offset and have propagating speeds in the order of a few m/s. Interestingly, at frequency 0.01 to 0.5 Hz, there are three visible oscillating frequencies bands. As shown in Figure 5a & b, the oscillating frequencies increase with the increase of the low-frequency signal (absolute) amplitude. Compared with its low-frequency counterpart that propagates slowly along the fibre (Figure 5d & e), the oscillating signals are spatially random, as we did not observe clear propagations in the space-time plot or f-k domain in Figure S2.

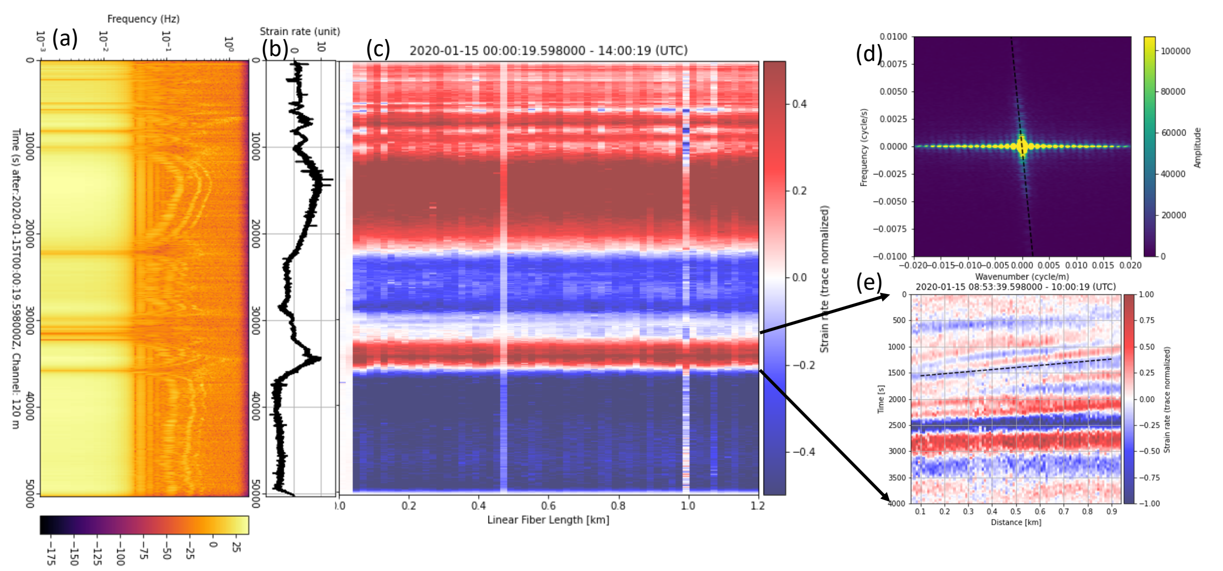


*Figure 5. Low frequency signals recorded by DAS. (a) spectrogram of the signal of (b) for a 100-second sliding window and 90% overlapping. (b) is 14 hours of continuous DAS recording, after a low pass filter and a 2 Hz resampling, at one DAS channel at 120 m. (c) Image plot of all DAS channels. (d) f-k transform of the 14 hours DAS data. © a 4000-second zoom-in as indicated.*

We suspect that this noise relates to atmospheric temperature variations, as the optical fibre was just slightly covered with snow. A study by Ide et al. (2021) suggest temperature variation might dominate the low-frequency part of DAS beyond 100 s. In addition, wind may be the source of the oscillations from 0.01 to 0.5 Hz, as it is expected to correlate with air pressure and temperature. Moreover, in the CCs (Figure 6b), we also see the strain signal of a moving marker-flag driven by the wind, although that signal is higher in frequency (9 Hz). Further investigation on this signal should be of interest for meteorology applications, but it is beyond the scope of this study.

## 2.2 Choice of Virtual Source: DAS versus Geophone

We initially obtain a DAS interferogram image through linearly stacking 2-minute CCs over the entire recording period of 5 days. We produce two different interferograms, the first uses the 600th DAS channel as a virtual source (Figure 6a), while the second takes the vertical component of a co-located geophone (at offset ~570 m) as the virtual source (Figure 6b). The CCs based on the DAS reference channel are noisy and the seismic responses, especially the lower frequency part, are faint. In contrast, the geophone virtual source produces an interferogram with a clear seismic signal.

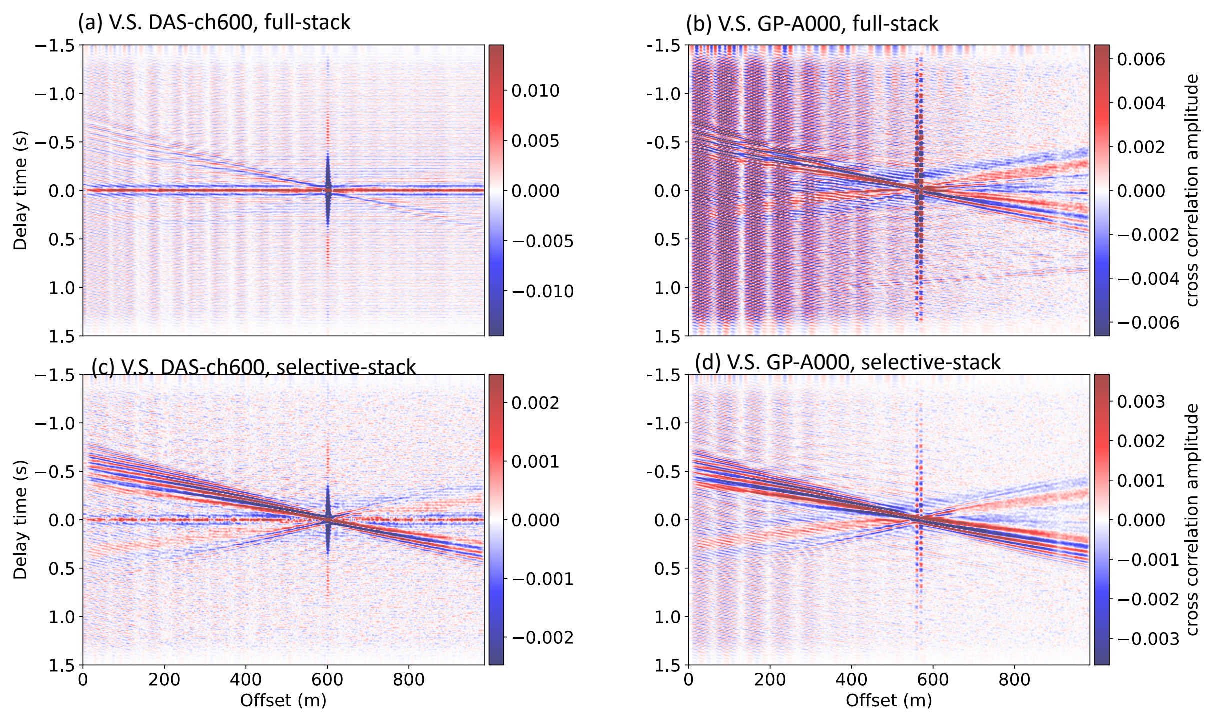


*Figure 6. (a) Stacked cross-correlations, a virtual shot gather, with a virtual source at DAS channel at 600 m. (b) Same as (a) but with a virtual source at a geophone (A000) located close to channel 550m. (c) Selective-stacked CCs for the same data as (a). (d) Selective-stacked CCs for the same data as (b)*

Considering the geophone virtual source derived CCs (Figure 6b), lower frequency seismic signals are observed travelling both forward (from 0 offset to large offset) and backward with an apparent velocity around 1.7 km/s. The higher frequency responses travel primarily in the forward direction and clear dispersion is observed; the higher frequency signals have a steeper slope, which indicates a slower velocity. The high frequency oscillating signal presenting at offset 0 to 600 m are due to a strong harmonic signal at 33.3 Hz generated by the petrol generator. The strong noise (9 Hz) around 560 and 570 m of the DAS channel is probably strain produced by moving of the poles of 2 marker-flags (used to indicate the location of the geophones) driven by wind. Since this signal is very localised it does not influence further analyses.

Although the geophone system measures particle velocity and DAS measures strain rate, combining their recordings has improved the resulting seismic response. We suspect this is due to the instrument noise on DAS channels having a harmful impact on the CCs. Firstly, we can see clear horizontal bands in Figure 6a which are most dominant at t = 0, and therefore indicates that the instrument noise on each DAS channel is not independent. This is likely due to the nature of DAS measurement that senses the entire cable with a single interrogator unit. When a geophone is used as the virtual source, this breaks the coherency of instrument noise, and thus the linear stacking is unharmful. Secondly, we observe that the dominant noise contributing to the seismic responses is transient, therefore a large number of CCs derived from a DAS virtual source contain only instrument noise. The correlation between vertical particle velocity (instrument response not corrected) and horizontal strain rate produces a phase shift on the CCs, which could be corrected by a second-order cross-correlation. Since, in this study, only apparent velocities (slope of in the time-offset plot) are used, no correction is needed.

## 2.3 Selective Stacking of Transient Noise

To improve the quality of the final interferogram image, previous studies have introduced more sophisticated techniques of stacking CCs, such as phase-weighted stacking (Schimmel et al., 2011; Schimmel & Paulssen, 1997) and SNR-weighted stacking (Cheng et al., 2015), or data selection (Dou et al., 2017; Zhou & Paulssen, 2020). Phase-weighted stacking suppresses incoherent noise among two CCs and has several advantages over a standard linear stack (Dou et al., 2017). The approach, however, assumes that noise is a continuous and coherent signal on every time span of CCs. Apart from the harmonic generator noise, most of the seismic signals recorded in our dataset are transient in nature. SNR-weighted stacking is based on the SNR of CCs and has been shown to perform well for anthropogenic seismic noises above 2 Hz, which are often transient and spatially variable (Cheng et al., 2015). For our 2-minute CCs, we find some signals have very low SNR when looking at individual channels which would be smeared (down-weighted by low SNR ratio) applying this method. Therefore, we take another approach, that is, selective stacking, where we stack selected CCs based on certain criteria. Previous studies have implemented selective stacking based on SNR (Olivier et al., 2015), or based on signal apparent velocity from beamforming analysis (Vidal et al., 2014).

In this paper, we choose to select a virtual shot gather of CCs based on the maximal amplitude on the tau-p domain (slant-stack, Figure 7) (Diebold & Stoffa, 1981), after a bandpass from 3 to 25 Hz. We select signals with their highest amplitude larger than 0.0014 (CC coefficient), located at delay time close to zero ($0 \pm 0.05$ s), and with an apparent velocity smaller than 2500 m/s (slowness < -0.4 or > 0.4 s/km). As shown in Figure 7a, the maximal amplitude is 0.00098, although at delay time around 0, thus is not selected. The strong signal in Figure 7c is selected.

These two criteria allow virtual shot gathers containing surface wave signals to be selected. Of the 3068 (5 days with few hours of data loss) 2-minute CCs, 453 time periods met the search criterion and were linearly stacked. The selective-stacked CCs are presented in Figure 6c & d, which show higher SNR of seismic responses compared to the fully stacked CCs (Figure 6a & b). Although the coherent instrument noise still presents in the selective-stacked CCs, for a DAS virtual source (Figure 6c), the seismic response is clearer since a large chunk of pure instrument noise is removed.

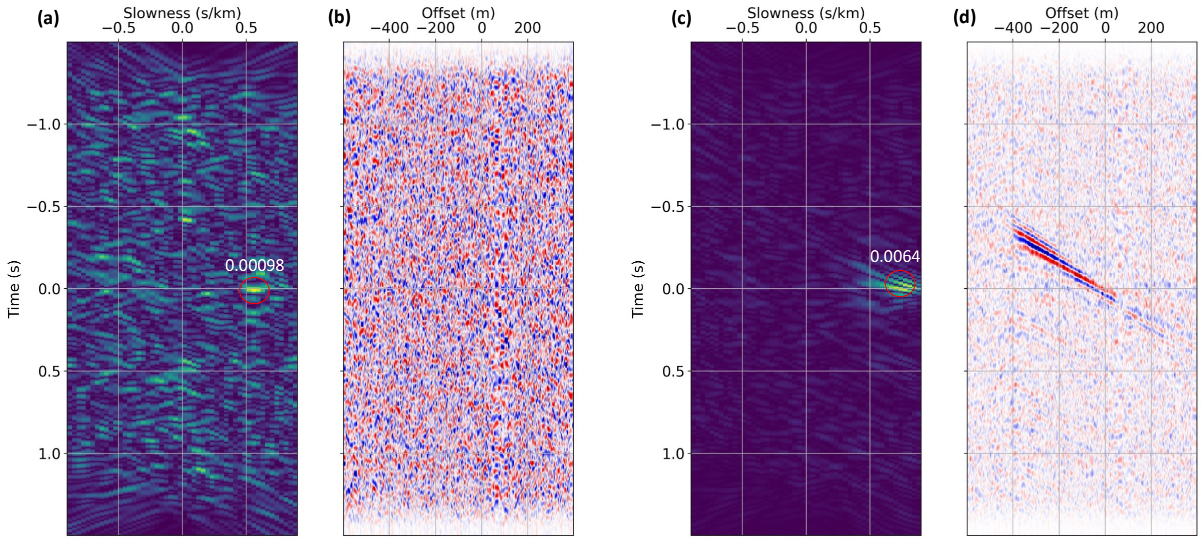


*Figure 7. (a, b) Example of a 'noisy' CC, with Tau-p domain plot in (a) the CCs in panel (b). (c, d) Example of a 'signal' CC, with Tau-p domain plot in (c) and CCs in panel (d). Peak amplitudes are indicated in the tau-p domain.*

Combining a geophone virtual source and selective stacking (Figure 6d), we achieve the best quality CCs for this dataset.

## 3 Dispersion and 1D velocity structure

### 3.1 Dispersion Analysis

We create dispersion curves for both the active and passive datasets using a frequency wavenumber (f-k) transform after applying a Hann window in both the time and space dimension. After applying the f-k transform, we stack the positive and negative parts of the K domain to further enhance the signal. These f-k domain plots (Figure S2) are then converted to the frequency–velocity domain as shown in Figure 8. Multiple modes of Rayleigh waves are presented in both datasets, but for simplicity, only the fundamental mode dispersion curve is extracted by picking the local maximal amplitude. The passive dataset contains lower frequency content and its dispersion curve is well constrained down to 3 Hz (Figure 8a). At around 33.3 Hz, there is a small but sharp reversal of velocity which is due to the near-constant wavenumber (Figure S2) of the strong noise observed at 33.3 Hz. This strong signal causes spectral leakage in fast Fourier transforms (FFT) even though a Hann window taper was applied before the FFT. However, since the frequency range is small it does not influence our inversion.

The dataset of 21 (2 shots for every 50 m) active surveys are processed as follows: First, for each shot gather, DAS channels are split into two segments at the location defined by the active source. Second, an f-k transform is applied to both segments. Third, negative wavenumbers are flipped and stacked with the positive part. Last, all shot gathers are stacked in the f-k domain. From Figure 8b, we see that the stacked active shots contain signals mostly beyond 10 Hz with dispersion most stable between 15 and 50 Hz. This is likely due to the lack of low-frequency energy generated by the hammer and plate source, compared to ambient seismic noise. In general, there is strong agreement from 15 to 50 Hz, between the dispersion curves from CCs and from shot gathers. This provides us with confidence that the methods adopted when producing the ANI interferogram are appropriate.

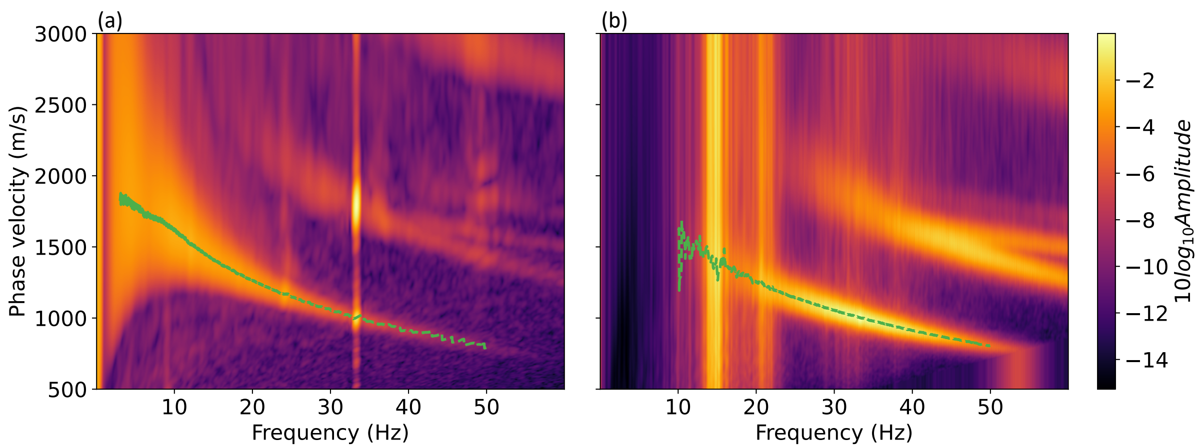


*Figure 8. (a) Extracting dispersion curve from the frequency-velocity domain of stacked CCs. (b) Dispersions obtained from stacked shot gathers in the f-k domain.*

### 3.2 Velocity Inversion

Most previous surface wave inversion studies treat the subsurface as a layered model with either fixed or variable layer thickness, for two-station (Yudistira et al., 2017) or multi-station (Cheng et al., 2015; Xia et al., 1999) surveys. The glacier firn layer is defined as a layer with continuous metamorphism of snow to ice. The continuous metamorphism results in a smooth increase of P and S velocity as a function of depth (King & Jarvis, 2007; Schlegel et al., 2019), until near-constant beneath ~100 m at RIS (Figure 1a). Due to these characteristics of the firn layer, instead of using a layered model with few layers and large thickness, we approach a near-continuous model with 100 layers, with each layer of thickness 1 m, except the bottom layer which represents a half-space.

To simulate the phase velocity dispersion of the Rayleigh wave, we use the Python package disba (Luu, 2021), which translated from the well-adapted Fortran program surf96 from Computer Programs in Seismology (Herrmann, 2013). With a 100-layer model, we significantly increase the number of variables and the non-uniqueness of the inversion. A Gaussian-Newton inversion procedure is applied using the package pyGimli (Rücker et al., 2017), with the regularization lambda to be 20, and a predefined relative error of 10% to prevent overfitting. The large relative error and regularization also mean we are finding a solution that is close to the starting model.

We use a smoothed firn layer P-wave velocity profile and constant Vp/Vs=1.95 (Smith, 2015) as our starting model (Figure 10). As shown in Figure 9, the starting model has in general consistent phase velocity with the data. But especially at higher frequencies, the starting model has lower phase velocity than the data, which indicates the starting model is underestimating at a shallower depth.

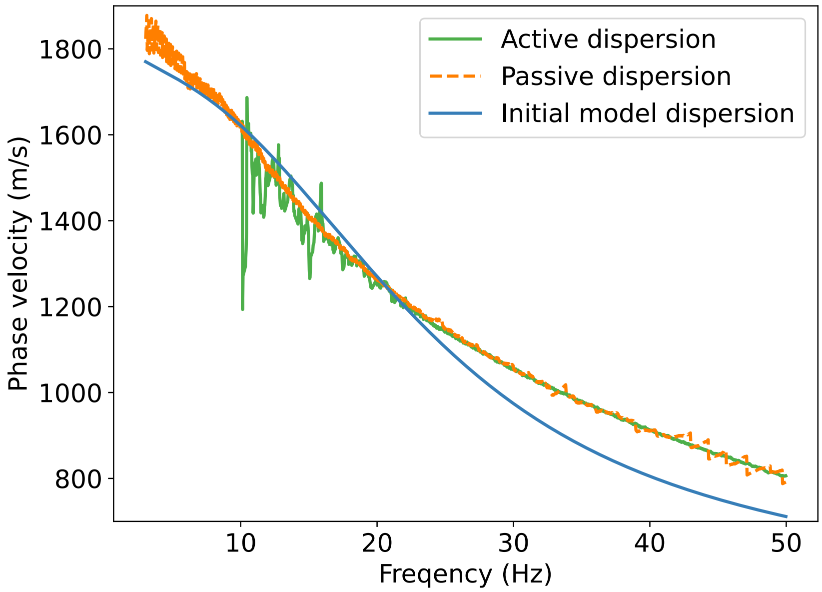


*Figure 9. Observed dispersion curves from selective stacked cross-correlations (CCs), active shot gather, and modelled dispersion from the initial Vs model.*

To capture the uncertainty in the data, we inverted each dispersion curve measured from every 50 (out of 453) selected 2-minute CCs and 3 virtual sources with the 3 collocated geophones (Figure S3). This produced 27 independent inversions of S-wave velocity, then, a probability density function (PDF) has been calculated over every layer. The amplitudes of PDFs are presented as greyscale in (Figure 10a). The maximal point of PDFs, for each layer, represents a Vs model (Vs_1 in Figure 10a). Alternatively, a Vs (Vs_2 in Figure 10a) is directly inverted from fully stacked CCs (all 453 time periods) and 3 virtual sources.

As highlighted in Figure 10a, the Vs_1 profile is smoother than Vs_2 and the two profiles differ marginally at all depths below 12 m, which further indicates uncertainties of the final models. To verify the inversions, we compare them with an S-wave velocity model produced by taking a P-wave velocity model from the standard refraction survey (Fig. 1c, 9a) and assuming a constant Vp/Vs ratio 1.95 (Smith et al., 2015). In general, our two Vs models agree with the standard profile down to 80 m depth. Below 80 m depth, our models suggest a slightly steeper increase in velocity compared to the standard refraction results, and reaches up to 2100 m/s. In both our Vs models and the standard model, we see a clear gradient increase (a rate of velocity change decrease) at around 12 m depth, which is similar to the densification observation and modelled by the regional atmospheric climate model by van den Broeke (2008), across West Antarctica.

A sensitivity analysis is done at discrete frequencies (3, 6, 10, 20, 40 Hz) as shown in (Figure 10b) using the standard firn layer model, indicating that the highest sensitivity of most signals (> 20 Hz) is over 0 to 40 m depth. Signals below 10 Hz have greater sensitivity over the lower part of the model. Below 6 Hz, the Rayleigh wave is dominantly sensitive to the lowermost layer of our model, which is assumed to be a half-space.

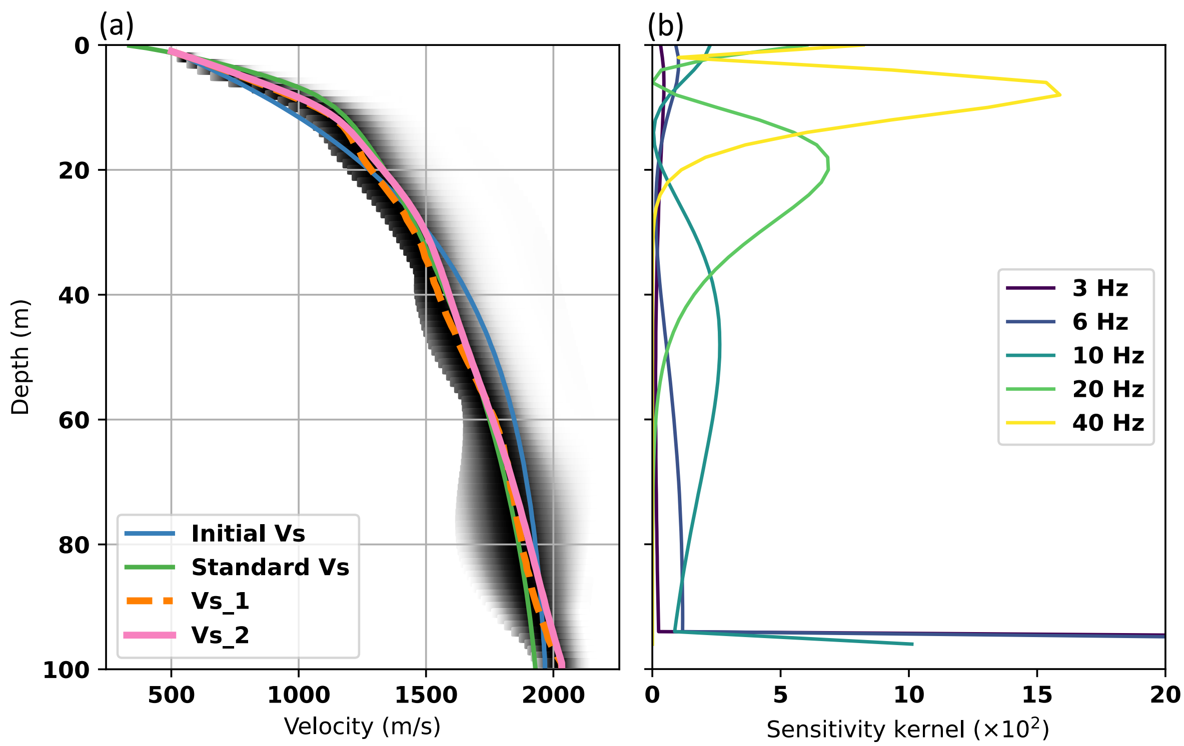


*Figure 10. (a) Two Inverted Vs models, Vs_1 from maximal PDF (greyscale) and Vs_2 from direct inversion of a fully selective stacked CCs virtual shot gather. The initial Vs model used in the inversion is in blue and for comparison, the Vs profile derived from the standard Vp refraction experiment is in green. (b) Sensitivity kernel calculated from the inverted model Vs_1.*

### 3.3 Is the firn layer seismically anisotropic?

Strong azimuthal anisotropy has been reported at RIS by Smith et al. (2017) at RIS, with the fast S-wave direction perpendicular (90°) to the ice flow direction (IFD). Hudson, Baird, et al. (2021) also observed strong shear wave splitting in icequake signals recorded by DAS. However, neither study provides a constraint on the depth distribution of the anisotropic ice, as the measurements integrate over the whole wave path from the icequake hypocentre (ice-bed interface) to surface receivers.

We investigate the feasibility of imaging anisotropy with surface waves retrieved from a different azimuth on CCs. For this, we use a DAS array that had been arranged into a triangular configuration and assume a laterally homogenous firn layer. As shown in Figure 11-a, we take two segments of the triangle array (channel 50-250 and channel 670-870). We chose channels 670-870, with a larger distance to the generator, to keep the influence of apparent velocity to be small. With virtual sources at DAS channels 150 and 750, respectively, we calculate and selectively stack 2-minute CCs for each segment. A higher selection threshold of 0.01 is chosen as the DAS CCs are in general of higher amplitude than DAS-geophone CCs. Dispersion curves of the 2 segments are then calculated from the f-k domain, as it is treated in the linear-array study. From Figure 11b, we can see that the two dispersion curves are in general near overlapping with each other, from 10 to 27 Hz. Above 27 Hz the 30° IFD curve indicates a slightly higher phase velocity, but the difference is small compared with the noise. It might also suggest heterogeneity in the near shallow firn, which is more likely than deeper down when it has densified further. Thus, we conclude that the firn layer, above ~80 m depth (for the signals above 10 Hz), must be azimuthally isotropic, at least below the level of our resolution.

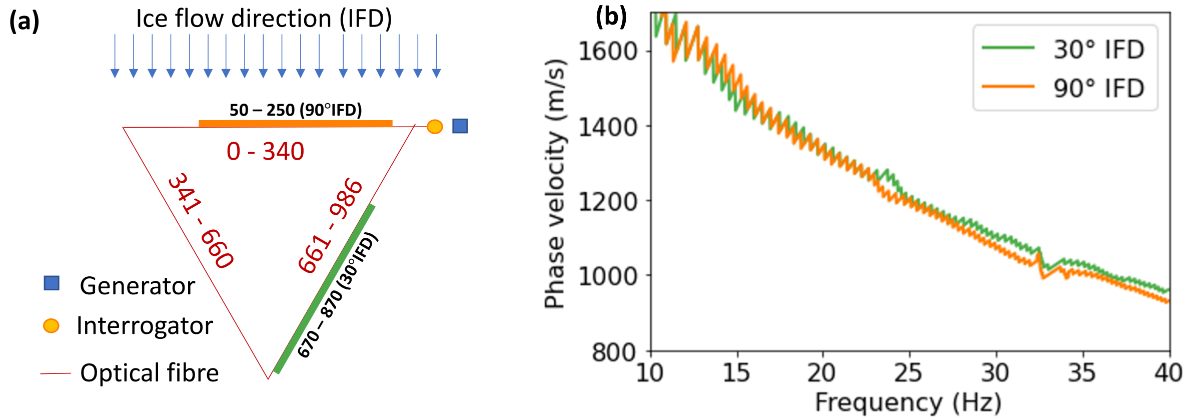


*Figure 11. (a) Schematic of the geometry of the triangle DAS array, with a loop of 986 m. The thick lines indicating two 200 m DAS segments have been used for the ANI study. (d) Dispersion curves were obtained from two segments.*

## 4 Discussions

In this study, we investigate the use of noise data recorded by DAS, deployed on RIS, West Antarctica, to obtain a high-resolution shear wave velocity profile of the firn. We compare CCs calculated over five days using a single DAS channel and 3 co-located geophones as the virtual sources and find a superior SNR with a co-located geophone. We argue that the coherence of instrument noise overall DAS channels would be harmful to cross-correlations for retrieving seismic response and introducing a geophone as a virtual source breaks down that coherence of the instrument noise. As a result of the Rayleigh wave elliptical particle motion, strong signals are retrieved from CCs between vertical component geophone data and horizontal component DAS data, with a notable phase shift (that could be removed by applying a secondary cross-correlation using a DAS channel as a virtual source instead). Based on our results we argue that deploying DAS together with conventional seismic instruments (hybrid instrumentation) would open more opportunities. This is consistent with previous studies by (Yu et al., 2019), who combined seismometer and DAS for calculating receiver function and also surface wave dispersion, Lindsey et al. (2020a) and van den Ende & Ampuero (2021), who use a seismometer to convert strain to particle velocity or calibrating that conversion, and Spica, Perton, et al. (2020) who combine DAS and a seismometer to apply the H/V method.

Selective stacking is applied to improve CCs, by selecting only virtual shot gathers that have slant-stacked correlation coefficients larger than 0.0014 around 0 delay time(a manually chosen value will likely vary site by site) at a frequency range of 3 to 25 Hz, and have apparent velocity smaller than 2500 m/s. Only 453 out of 3068 2-minute periods are selected and stacked for shear wave inversions. With selective stacking, we eliminate a large chunk of data containing only instrument noises. The selected virtual shot gathers contain mostly high-frequency signals from the generator or transient low-frequency surface wave events. The generator sits in-line with the linear fibre optic cable array, 50 m away from the interrogator (Figure 11a), and produces a surface wave noise travelling along the fibre. The surface wave events are from the shear margin of RIS (Figure S4), which are different from basal icequakes and are suspected to be crevasse activity or ice fracture, are not homogeneously distributed, but generally in-line with the fibre optic cable. Additionally, given that the DAS is mostly sensitive to strain along the cable direction, signals travelling oblique to the cable might be recorded by vertical component geophones but not by DAS, which enhances the stationary seismic energy in CCs.

The dispersion curves obtained from the passive and active datasets show strong agreement over the frequency range 10 to 50 Hz. While the hammer & plate source surveys reach down to 10 Hz, it is most stable beyond 15 Hz, which could provide a reliable S velocity profile down to ~60 m (Figure 10). The use of noise extends the reliable measurement range down to 3 Hz, thanks to events with strong surface wave signals which are abundant from margins of RIS (Figure S4), which enable the inversion over the entire firn.

We did not observe microseism seismic noise that is dominating ambient noise on broadband seismometers from 0.01 to 1 Hz (Bensen et al., 2007). Previous studies with submarine DAS cables have recorded the microseism from 0.2 to 2 Hz (Sladen et al., 2019) and down to 0.5 Hz (Cheng et al., 2015; Spica, Nishida, et al., 2020). Some onshore studies also suggest the abundance of low-frequency noises with noise power spectrum analysis (Hudson, Kendall, et al., 2021; Lindsey et al., 2020a). It is, however, shown in our study that the dominating low-frequency noise from RIS, is not a seismic signal, and could instead be due to shallow cable burying and strong environment noise from temperature, pressure variation and wind, but also due to the higher instrument noise on DAS. It is also possible that the linear fibre is insensitive to microseism signals because of its propagation direction near perpendicular to the fibre.

The S-wave velocity profile obtained from this study fits well with the velocity profile derived from a standard refraction P-wave experiment (Smith et al., 2021) assuming a Vp/Vs ratio of 1.95 (Smith et al., 2015) at depths of 0 to 80 m. Below 80 m the profiles from the methods divergence, with higher Vs at depths greater than 80 m from the surface wave inversion. This may suggest a decrease of the Vp/Vs ratio at depth, or an increase in azimuthal anisotropy. However, at these depths, the reliability of the standard refraction results decreases due to the data offset limitation of ~1 km. Also, spatial heterogeneity cannot be ruled out as the surveys are not collocated. Nevertheless, the shape and form of the inverted Vs profiles shows extremely good agreement with the refraction survey, with both methods showing a velocity-depth gradient change at around 12 m. This feature of the velocity profile likely indicates the depth of the critical density, marking the transition between the first two stages of the densification process (Herron & Langway, 1980). Above this depth, the dominant compaction mechanism is grain settling and packing and exhibits the highest densification rate. Below this transition progression to pore close-off occurs with a lower rate of densification. The velocity-depth gradients above and below this depth agree with this interpretation. This agreement between the methods, reproducing the velocity gradient transition at similar depths is significant. The standard refraction WHB method uses a double exponential fit to the traveltimes which can force the presence of this gradient change when a simple polynomial fitting method may not. The results from noise interferometry and surface wave inversion, therefore, verify the assumption of the double exponential fitting step and provide an independent and robust measure of this critical density transition in the firn profile.

Furthermore, although standard refraction methods can be adapted to derive a Vs profile, with S wave sources and 3 component instruments (King & Jarvis, 2007; Kirchner & Bentley, 2013), in general, only Vp profiles are determined. Our measurement of Vs complements with Vp, without requiring additional S wave sources, which may lead to an improved understanding of the mechanical properties of the firn and their variation. Efforts were made to reproduce the standard P-wave refraction survey method using diving P-waves from a hammer and plate source with DAS recording. However, inherent to the DAS method, a combination of gauge length and spatial averaging results in steps immediately surrounding the shot location, producing a poorly constrained velocity profile.

Another potential benefit of the method presented here compared to the standard seismic refraction method is the capacity of the surface wave (passive or active) to image low-velocity layers (LVL) (Zhang et al., 2007). The seismic refraction method would fail in the presence of low-velocity layers as no rays will undergo critical refraction at the top of the LVL. This situation may arise where melt has occurred and refreezing produced ice lenses overlying lower velocity firn layers, as for example reported on the Larsen Ice Shelf (Ashmore et al., 2017).

With a triangular fibre optic array, we retrieve Rayleigh wave responses along direction 90° and 30° from the ice flow direction. We find no clear difference between the two dispersion curves from 10 to 40 Hz, which indicates azimuthal isotropy in the upper 80 m (the dominant sensitivity of this frequency band is the top 80 m (Figure 10b)). Studies by Smith et al. (2017) and Hudson, Baird, et al. (2021), however, observed strong anisotropy using icequake signals travelling from the ice column base to the surface. Thus, our observation of a near isotropic firn layer would suggest the anisotropic ice is present at greater depth.

## 5 Conclusions

In conclusion, taking advantage of the seismicity containing lower-frequency (2 – 10 Hz) surface wave signal from the shear margins of the ice stream, and the high-frequency noise from a petrol generator located on-site, we retrieved broadband (3 – 50 Hz) and stable CCs representing Rayleigh wave responses travelling along the DAS fibre. We show that the SNR improves when using a collocated geophone as the virtual source or selective stacking CCs which contains surface wave signal – determined from the tau-p domain. The Rayleigh wave dispersion curves are validated with active shot gathers. The dispersion curves are inverted to produce an S-wave velocity (Vs) profile of the firn layer, which shows good agreement with a standard Vp refraction derived model, including the depth to the critical density. No significant azimuthal anisotropy is observed in the upper 80 m, using 10 to 40 Hz signal, which suggests the top of the firn layer is not under deformation at our study site. Derivation of the Vs profile from surface wave, with either ambient noise interferometry or active shots, will complement the standard Vp profiles (often acquired from seismic refraction). Additionally, it will potentially allow investigation of the firn column where standard refraction methods fall in the presence of LVLs, such as on higher-latitude ice shelves.

## Acknowledgements

This work was funded by the UK's Department for Business, Energy and Industrial Strategy through the DigiMon ACT CCS project (project number 299622), and the NERC Collaborative Antarctic Science Scheme grant (grant number CASS-166). Fieldwork was undertaken as part of the BEAMISH Project (NERC AFI award numbers NE/G014159/1). We thank Silixa for the loan of an iDAS interrogator. Geophones were borrowed from the UK Geophysical Equipment Facility (GEF loan number 1111). Obspy (Krischer et al., 2015) is intensively used for data processing. Tau-p transform was performed with PyLops (Ravasi & Vasconcelos, 2020). Thomas Hudson, Sacha Lapins and Hanneke Paulssen are thanked for useful discussions.

## Open Research

7 hours of continuous DAS data (decimated to 10 m channel distance and 100 Hz sampling rate), and continuous geophones data (3 collocated geophone, A000, R102, R104, vertical component) have been made available through Zenodo (10.5281/zenodo.5927541), which could be used to reproduce this study.

## References

Ajo-Franklin, J. B., Dou, S., Lindsey, N. J., Monga, I., Tracy, C., Robertson, M., Rodriguez Tribaldos, V., Ulrich, C., Freifeld, B., Daley, T., & Li, X. (2019). Distributed Acoustic Sensing Using Dark Fiber for Near-Surface Characterization and Broadband Seismic Event Detection. *Scientific Reports*, *9*(1), 1328. https://doi.org/10.1038/s41598-018-36675-8

Alley, R. B. (1987). FIRN DENSIFICATION BY GRAIN-BOUNDARY SLIDING: A FIRST MODEL. *Journal de Physique (Paris), Colloque*, *48*(3). https://doi.org/10.1051/jphyscol:1987135

Ashmore, D. W., Hubbard, B., Luckman, A., Kulessa, B., Bevan, S., Booth, A., Munneke, P. K., O'Leary, M., Sevestre, H., & Holland, P. R. (2017). Ice and firn heterogeneity within Larsen C Ice Shelf from borehole optical televiewing. *Journal of Geophysical Research: Earth Surface*, *122*(5), 1139–1153. https://doi.org/10.1002/2016JF004047

Bensen, G. D., Ritzwoller, M. H., Barmin, M. P., Levshin, A. L., Lin, F., Moschetti, M. P., Shapiro, N. M., & Yang, Y. (2007). Processing seismic ambient noise data to obtain reliable broad-band surface wave dispersion measurements. *Geophysical Journal International*, *169*(3), 1239–1260. https://doi.org/10.1111/j.1365-246X.2007.03374.x

Booth, A. D., Christoffersen, P., Schoonman, C., Clarke, A., Hubbard, B., Law, R., Doyle, S. H., Chudley, T. R., & Chalari, A. (2020). Distributed Acoustic Sensing of Seismic Properties in a Borehole Drilled on a Fast-Flowing Greenlandic Outlet Glacier. *Geophysical Research Letters*, *47*(13). https://doi.org/10.1029/2020GL088148

Brisbourne, A. M., Kendall, M., Kufner, S. K., Hudson, T. S., & Smith, A. M. (2021). Downhole distributed acoustic seismic profiling at Skytrain Ice Rise, West Antarctica. *Cryosphere*, *15*(7), 3443–3458. https://doi.org/10.5194/tc-15-3443-2021

Butcher, A., Hudson, T., Kendall, J., Kufner, S., Brisbourne, A., & Stork, A. (2021). Radon transform-based detection of microseismicity on DAS networks: A case study from Antarctica. *EAGE GeoTech 2021 - 1st EAGE Workshop on Induced Seismicity*. https://doi.org/10.3997/2214-4609.202131039

Butcher, A., Stork, A. L., Verdon, J. P., Kendall, J. M., Plenkers, K., Booth, F., Boneham, M., & Koe, A. (2021). Evaluating rock mass disturbance within open-pit excavations using seismic methods: A case study from the Hinkley Point C nuclear power station. *Journal of Rock Mechanics and Geotechnical Engineering*, *13*(3). https://doi.org/10.1016/j.jrmge.2020.12.001

Cheng, F., Chi, B., Lindsey, N. J., Dawe, T. C., & Ajo-Franklin, J. B. (2021). Utilizing distributed acoustic sensing and ocean bottom fiber optic cables for submarine structural characterization. *Scientific Reports*, *11*(1). https://doi.org/10.1038/s41598-021-84845-y

Cheng, F., Xia, J., Xu, Y., Xu, Z., & Pan, Y. (2015). A new passive seismic method based on seismic interferometry and multichannel analysis of surface waves. *Journal of Applied Geophysics*, *117*, 126–135. https://doi.org/10.1016/j.jappgeo.2015.04.005

Correa, J., Freifeld, B. M., Revzner, R., Wood, T., Tertyshnikov, K., & Bona, A. (2018). Continuous DAS VSP monitoring using surface orbital vibrators: Field trials for optimal configuration at the CO2CRC Otway Project. *80th EAGE Conference and Exhibition 2018 Workshop Programme*, cp--00040. https://doi.org/10.3997/2214-4609.201801917

Craig, H., Horibe, Y., & Sowers, T. (1988). Gravitational Separation of Gases and Isotopes in Polar Ice Caps. *Science*, *242*(4886), 1675–1678. https://doi.org/10.1126/science.242.4886.1675

Cuffey, K. M., & Paterson, W. S. . B. (2010). Physics of Glaciers, Fourth Edition. In *The Physics of Glaciers*.

Diebold, J. B., & Stoffa, P. L. (1981). The traveltime equation, tau-p mapping, and inversion of common midpoint data. *Geophysics*, *46*(3). https://doi.org/10.1190/1.1441196

Dou, S., Lindsey, N., Wagner, A. M., Daley, T. M., Freifeld, B., Robertson, M., Peterson, J., Ulrich, C., Martin, E. R., & Ajo-Franklin, J. B. (2017). Distributed Acoustic Sensing for Seismic Monitoring of the Near Surface: A Traffic-Noise Interferometry Case Study. *Scientific Reports*, *7*(1). https://doi.org/10.1038/s41598-017-11986-4

He, X., Xie, S., Liu, F., Cao, S., Gu, L., Zheng, X., & Zhang, M. (2017). Multi-event waveform-retrieved distributed optical fiber acoustic sensor using dual-pulse heterodyne phase-sensitive OTDR. *Optics Letters*, *42*(3), 442. https://doi.org/10.1364/OL.42.000442

Herrmann, R. B. (2013). Computer programs in seismology: An evolving tool for instruction and research. *Seismological Research Letters*, *84*(6). https://doi.org/10.1785/0220110096

Herron, M. M., & Langway, C. C. (1980). Firn densification: an empirical model. *Journal of Glaciology*, *25*(93). https://doi.org/10.1017/S0022143000015239

Hollmann, H., Treverrow, A., Peters, L. E., Reading, A. M., & Kulessa, B. (2021). Seismic observations of a complex firn structure across the Amery Ice Shelf, East Antarctica. *Journal of Glaciology*, *67*(265), 777–787. https://doi.org/10.1017/jog.2021.21

Hudson, T. S., Baird, A. F., Kendall, J. M., Kufner, S. K., Brisbourne, A. M., Smith, A. M., Butcher, A., Chalari, A., & Clarke, A. (2021). Distributed Acoustic Sensing (DAS) for Natural Microseismicity Studies: A Case Study From Antarctica. *Journal of Geophysical Research: Solid Earth*, *126*(7). https://doi.org/10.1029/2020JB021493

Hudson, T. S., Kendall, J.-M., Kufner, S.-K., Brisbourne, A. M., & Smith, A. M. (2021). Distributed acoustic sensing (DAS) for microseismicity studies: A case study from Antarctica. *Submitted to JGR Solid Earth*.

Ide, S., Araki, E., & Matsumoto, H. (2021). Very broadband strain-rate measurements along a submarine fiber-optic cable off Cape Muroto, Nankai subduction zone, Japan. *Earth, Planets and Space*, *73*(1). https://doi.org/10.1186/s40623-021-01385-5

King, E. C., & Jarvis, E. P. (2007). Use of Shear Waves to Measure Poisson's Ratio in Polar Firn. *Journal of Environmental and Engineering Geophysics*, *12*(1), 15–21. https://doi.org/10.2113/JEEG12.1.15

Kirchner, J. F., & Bentley, C. R. (1979). Seismic Short-Refraction Studies on the Ross Ice Shelf, Antarctica. *Journal of Glaciology*, *24*(90), 313–319. https://doi.org/10.3189/S0022143000014830

Kirchner, J. F., & Bentley, C. R. (2013). *RIGGS III: Seismic Short-Refraction Studies Using an Analytical Curve-Fitting Technique* (pp. 109–126). https://doi.org/10.1029/AR042p0109

Krischer, L., Megies, T., Barsch, R., Beyreuther, M., Lecocq, T., Caudron, C., & Wassermann, J. (2015). ObsPy: a bridge for seismology into the scientific Python ecosystem. *Computational Science & Discovery*, *8*(1), 014003. https://doi.org/10.1088/1749-4699/8/1/014003

Kufner, S., Brisbourne, A. M., Smith, A. M., Hudson, T. S., Murray, T., Schlegel, R., Kendall, J. M., Anandakrishnan, S., & Lee, I. (2021). Not all Icequakes are Created Equal: Basal Icequakes Suggest Diverse Bed Deformation Mechanisms at Rutford Ice Stream, West Antarctica. *Journal of Geophysical Research: Earth Surface*, *126*(3). https://doi.org/10.1029/2020JF006001

Lellouch, A., Yuan, S., Spica, Z., Biondi, B., & Ellsworth, W. L. (2019). Seismic Velocity Estimation Using Passive Downhole Distributed Acoustic Sensing Records: Examples From the San Andreas Fault Observatory at Depth. *Journal of Geophysical Research: Solid Earth*, *124*(7), 6931–6948. https://doi.org/10.1029/2019JB017533

Lindner, F., Laske, G., Walter, F., & Doran, A. K. (2019). Crevasse-induced Rayleigh-wave azimuthal anisotropy on Glacier de la Plaine Morte, Switzerland. *Annals of Glaciology*, *60*(79), 96–111. https://doi.org/10.1017/aog.2018.25

Lindsey, N. J., Rademacher, H., & Ajo-Franklin, J. B. (2020a). On the Broadband Instrument Response of Fiber-Optic DAS Arrays. *Journal of Geophysical Research: Solid Earth*, *125*(2), 1–16. https://doi.org/10.1029/2019JB018145

Lindsey, N. J., Rademacher, H., & Ajo-Franklin, J. B. (2020b). On the Broadband Instrument Response of Fiber-Optic DAS Arrays. *Journal of Geophysical Research: Solid Earth*, *125*(2), e2019JB018145. https://doi.org/10.1029/2019JB018145

Lior, I., Mercerat, E. D., Rivet, D., Sladen, A., & Ampuero, J.-P. (2021). *Imaging an Underwater Basin and its Resonance Modes using Optical Fiber Distributed Acoustic Sensing*. https://doi.org/https://doi.org/10.31223/X5XK8P

Lior, I., Sladen, A., Rivet, D., Ampuero, J. P., Hello, Y., Becerril, C., Martins, H. F., Lamare, P., Jestin, C., Tsagkli, S., & Markou, C. (2021). On the Detection Capabilities of Underwater Distributed Acoustic Sensing. *Journal of Geophysical Research: Solid Earth*, *126*(3), 1–20. https://doi.org/10.1029/2020JB020925

Luu, K. (2021). *disba: Numba-accelerated computation of surface wave dispersion*. https://doi.org/https://doi.org/10.5281/zenodo.3987395

Mateeva, A., Lopez, J., Chalenski, D., Tatanova, M., Zwartjes, P., Yang, Z., Bakku, S., Vos, K. de, & Potters, H. (2017). 4D das VSP as a tool for frequent seismic monitoring in deep water. *Leading Edge*, *36*(12), 995–1000. https://doi.org/10.1190/tle36120995.1

Murray, T., Smith, A. M., King, M. A., & Weedon, G. P. (2007). Ice flow modulated by tides at up to annual periods at Rutford Ice Stream, West Antarctica. *Geophysical Research Letters*, *34*(18), L18503. https://doi.org/10.1029/2007GL031207

Olivier, G., Brenguier, F., Campillo, M., Lynch, R., & Roux, P. (2015). Body-wave reconstruction from ambient seismic noise correlations in an underground mine. *GEOPHYSICS*, *80*(3). https://doi.org/10.1190/geo2014-0299.1

Ravasi, M., & Vasconcelos, I. (2020). PyLops—A linear-operator Python library for scalable algebra and optimization. *SoftwareX*, *11*, 100361. https://doi.org/10.1016/j.softx.2019.100361

Riverman, K. L., Alley, R. B., Anandakrishnan, S., Christianson, K., Holschuh, N. D., Medley, B., Muto, A., & Peters, L. E. (2019). Enhanced Firn Densification in High-Accumulation Shear Margins of the NE Greenland Ice Stream. *Journal of Geophysical Research: Earth Surface*, *124*(2), 365–382. https://doi.org/10.1029/2017JF004604

Rodríguez Tribaldos, V., & Ajo-Franklin, J. B. (2021). Aquifer Monitoring Using Ambient Seismic Noise Recorded With Distributed Acoustic Sensing (DAS) Deployed on Dark Fiber. *Journal of Geophysical Research: Solid Earth*, *126*(4), 1–20. https://doi.org/10.1029/2020jb021004

Rodríguez Tribaldos, V., Ajo-Franklin, J., Dou, S., Lindsey, N., Ulrich, C., Robertson, M., Freifeld, B., Daley, T., Monga, I., & Tracy, C. (2019). *Surface Wave Imaging using Distributed Acoustic Sensing Deployed on Dark Fiber: Moving Beyond High Frequency Noise*. https://doi.org/10.31223/OSF.IO/JB2NA

Rücker, C., Günther, T., & Wagner, F. M. (2017). pyGIMLi: An open-source library for modelling and inversion in geophysics. *Computers & Geosciences*, *109*, 106–123. https://doi.org/10.1016/j.cageo.2017.07.011

Schimmel, M., & Paulssen, H. (1997). Noise reduction and detection of weak, coherent signals through phase-weighted stacks. *Geophysical Journal International*, *130*(2), 497–505. https://doi.org/10.1111/j.1365-246X.1997.tb05664.x

Schimmel, M., Stutzmann, E., & Gallart, J. (2011). Using instantaneous phase coherence for signal extraction from ambient noise data at a local to a global scale. *Geophysical Journal International*, *184*(1), 494–506. https://doi.org/10.1111/j.1365-246X.2010.04861.x

Schlegel, R., Diez, A., Löwe, H., Mayer, C., Lambrecht, A., Freitag, J., Miller, H., Hofstede, C., & Eisen, O. (2019). Comparison of elastic moduli from seismic diving-wave and ice-core microstructure analysis in Antarctic polar firn. *Annals of Glaciology*, *60*(79), 220–230. https://doi.org/10.1017/aog.2019.10

Sergeant, A., Chmiel, M., Lindner, F., Walter, F., Roux, P., Chaput, J., Gimbert, F., & Mordret, A. (2020). On the Green's function emergence from interferometry of seismic wave fields generated in high-melt glaciers: implications for passive imaging and monitoring. *The Cryosphere*, *14*(3), 1139–1171. https://doi.org/10.5194/tc-14-1139-2020

Shapiro, N. M., & Campillo, M. (2004). Emergence of broadband Rayleigh waves from correlations of the ambient seismic noise. *Geophysical Research Letters*, *31*(7), 8–11. https://doi.org/10.1029/2004GL019491

Shapiro, N. M., Campillo, M., Stehly, L., & Ritzwoller, M. H. (2005). High-resolution surface-wave tomography from ambient seismic noise. *Science*, *307*(5715), 1615–1618.

Shepherd, A., Ivins, E. R., Geruo, A., Barletta, V. R., Bentley, M. J., Bettadpur, S., Briggs, K. H., Bromwich, D. H., Forsberg, R., Galin, N., Horwath, M., Jacobs, S., Joughin, I., King, M. A., Lenaerts, J. T. M., Li, J., Ligtenberg, S. R. M., Luckman, A., Luthcke, S. B., … Zwally, H. J. (2012). A reconciled estimate of ice-sheet mass balance. *Science*, *338*(6111). https://doi.org/10.1126/science.1228102

Slichter, L. B. (1932). The Theory of the Interpretation of Seismic Travel-Time Curves in Horizontal Structures. *Physics*, *3*(6), 273–295. https://doi.org/10.1063/1.1745133

Smith, A. M. (1997). Variations in basal conditions on Rutford Ice Stream, West Antarctica. *Journal of Glaciology*, *43*(144), 245–255. https://doi.org/10.3189/S0022143000003191

Smith, A. M., Anker, P. G. D., Nicholls, K. W., Makinson, K., Murray, T., Rios-Costas, S., Brisbourne, A. M., Hodgson, D. A., Schlegel, R., & Anandakrishnan, S. (2021). Ice stream subglacial access for ice-sheet history and fast ice flow: the BEAMISH Project on Rutford Ice Stream, West Antarctica and initial results on basal conditions. *Annals of Glaciology*, *62*(85–86), 203–211. https://doi.org/10.1017/aog.2020.82

Smith, E. C., Baird, A. F., Kendall, J. M., Martín, C., White, R. S., Brisbourne, A. M., & Smith, A. M. (2017). Ice fabric in an Antarctic ice stream interpreted from seismic anisotropy. *Geophysical Research Letters*, *44*(8), 3710–3718. https://doi.org/10.1002/2016GL072093

Smith, E. C., Smith, A. M., White, R. S., Brisbourne, A. M., & Pritchard, H. D. (2015). Mapping the ice-bed interface characteristics of Rutford Ice Stream, West Antarctica, using microseismicity. *Journal of Geophysical Research: Earth Surface*, *120*(9), 1881–1894. https://doi.org/10.1002/2015JF003587

Snieder, R., & Larose, E. (2013). Extracting Earth's Elastic Wave Response from Noise Measurements. *Annual Review of Earth and Planetary Sciences*, *41*(1), 183–206. https://doi.org/10.1146/annurev-earth-050212-123936

Spica, Z. J., Nishida, K., Akuhara, T., Pétrélis, F., Shinohara, M., & Yamada, T. (2020). Marine Sediment Characterized by Ocean-Bottom Fiber-Optic

Seismology. *Geophysical Research Letters*, *47*(16), e2020GL088360. https://doi.org/10.1029/2020GL088360

Spica, Z. J., Perton, M., Martin, E. R., Beroza, G. C., & Biondi, B. (2020). Urban Seismic Site Characterization by Fiber-Optic Seismology. *Journal of Geophysical Research: Solid Earth*, *125*(3), 1–14. https://doi.org/10.1029/2019JB018656

van den Broeke, M. (2005). Strong surface melting preceded collapse of Antarctic Peninsula ice shelf. *Geophysical Research Letters*, *32*(12), 1–4. https://doi.org/10.1029/2005GL023247

van den Broeke, M. (2008). Depth and Density of the Antarctic Firn Layer. *Arctic, Antarctic, and Alpine Research*, *40*(2), 432–438. https://doi.org/10.1657/1523-0430(07-021)

van den Ende, M. P. A., & Ampuero, J. P. (2021). Evaluating seismic beamforming capabilities of distributed acoustic sensing arrays. *Solid Earth*, *12*(4), 915–934. https://doi.org/10.5194/se-12-915-2021

Vidal, C. A., Draganov, D., van der Neut, J., Drijkoningen, G., & Wapenaar, K. (2014). Retrieval of reflections from ambient noise using illumination diagnosis. *Geophysical Journal International*, *198*(3), 1572–1584. https://doi.org/10.1093/gji/ggu164

Walter, F., Gräff, D., Lindner, F., Paitz, P., Köpfli, M., Chmiel, M., & Fichtner, A. (2020). Distributed acoustic sensing of microseismic sources and wave propagation in glaciated terrain. *Nature Communications*, *11*(1). https://doi.org/10.1038/s41467-020-15824-6

Walter, F., Roux, P., Roeoesli, C., Lecointre, A., Kilb, D., & Roux, P. F. (2015). Using glacier seismicity for phase velocity measurements and Green's function retrieval. *Geophysical Journal International*, *201*(3). https://doi.org/10.1093/gji/ggv069

Williams, E. F., Fernández-Ruiz, M. R., Magalhaes, R., Vanthillo, R., Zhan, Z., González-Herráez, M., & Martins, H. F. (2019). Distributed sensing of microseisms and teleseisms with submarine dark fibers. *Nature Communications*, *10*(1), 1–11. https://doi.org/10.1038/s41467-019-13262-7

Xia, J., Miller, R. D., & Park, C. B. (1999). Estimation of near-surface shear-wave velocity by inversion of Rayleigh waves. *GEOPHYSICS*, *64*(3), 691–700. https://doi.org/10.1190/1.1444578

Yu, C., Zhan, Z., Lindsey, N. J., Ajo-Franklin, J. B., & Robertson, M. (2019). The Potential of DAS in Teleseismic Studies: Insights From the Goldstone Experiment. *Geophysical Research Letters*, *46*(3), 1320–1328. https://doi.org/10.1029/2018GL081195

Yudistira, T., Paulssen, H., & Trampert, J. (2017). The crustal structure beneath The Netherlands derived from ambient seismic noise. In *Tectonophysics* (Vol. 721, Issue 77). https://doi.org/10.1016/j.tecto.2017.09.025

Zhang, X., Paulssen, H., Lebedev, S., & Meier, T. (2007). Surface wave tomography of the Gulf of California. *Geophysical Research Letters*, *34*(15). https://doi.org/10.1029/2007GL030631

Zhou, W., & Paulssen, H. (2020). Compaction of the Groningen gas reservoir investigated with train noise. *Geophysical Journal International*, *223*(2), 1327–1337. https://doi.org/10.1093/gji/ggaa364

*JGR Earth Surface*

Supporting Information for

# Ambient Seismic Recordings and Distributed Acoustic Sensing (DAS): Imaging the firn layer on Rutford Ice Stream, Antarctica

Wen Zhou[1], Antony Butcher[1], Alex Brisbourne[2], Sofia-Katerina Kufner[2], J-Michael Kendall[3], Anna Stork[4]

[1]University of Bristol, BS8 1TH, Bristol, UK

[2]British Antarctic Survey, CB3 0ET, Cambridge, UK

[3]University of Oxford, OX1 2JD, Oxford, UK

[4]Silixa, WD6 3SN, Borehamwood, UK

Corresponding author: Wen Zhou (wz18709@bristol.ac.uk)

## Contents of this file



## Introduction

A comparison of noise interferometry and frequency-wavenumber (f-k) domain stacking is provided in Text S1 and Figure S1. DAS noise from 0.01 to 1 Hz is shown in Figure S2. f-k transform of cross-correlations in Figure S3. Variations of dispersions curves in Figure S4. Located shear margin seismic events using the geophone array in Figure S5.

### Text S1. Noise interferometry vs. raw data f-k transform

Both cross-correlation (CC, with spectral whitening, thus equivalent to cross coherent) and deconvolution (DC) are applied to retrieve impulse responses, with a virtual source at a 10 m distance. As shown in Figure S1 a and b, DC supressed the generator oscillations at 33 and 66 Hz, and produce a cleaner image, while CC preserves the oscillations. From the f-k transform in Figure S1 c and d, we also learn that DC suppressessupresses the higher modes, and at the same time produces a less shaper fundamental mode. Frequency leakages are observed around 33 and 66 Hz, on both CC and DC f-k plots, but not for the raw data f-k transform.

Compared with noise interferometry processes, the stacked raw data f-k transform (Figure S1 e) can also be used forto dispersion, as in this case study, the noise source is stable likely from the generator, and in-line with the linear fibre.

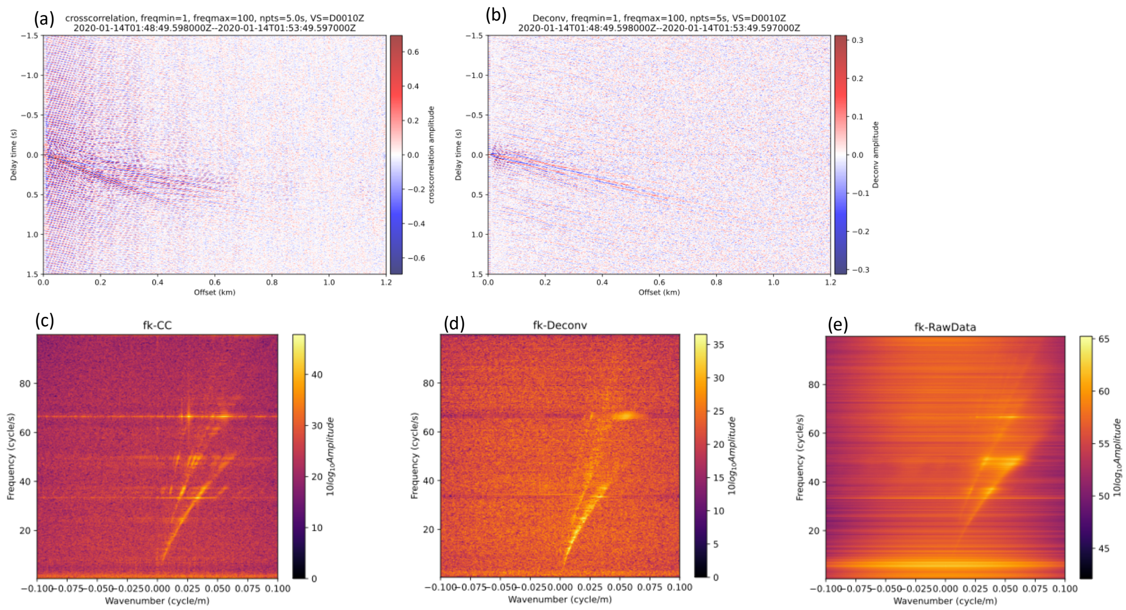


**Figure S1. (a) Cross-correlation interferometry using the 200-second signal as shown in** Error! Reference source not found.**, with a virtual source at channel 10 m. (b) Deconvolution interferometry using the same signal and virtual source, with water-level 1e-5. (c) F-K transform of the CCs. (d) F-K transform of the deconvolutions. (e) stacked F-K transform of the raw data, without interferometry processing.**

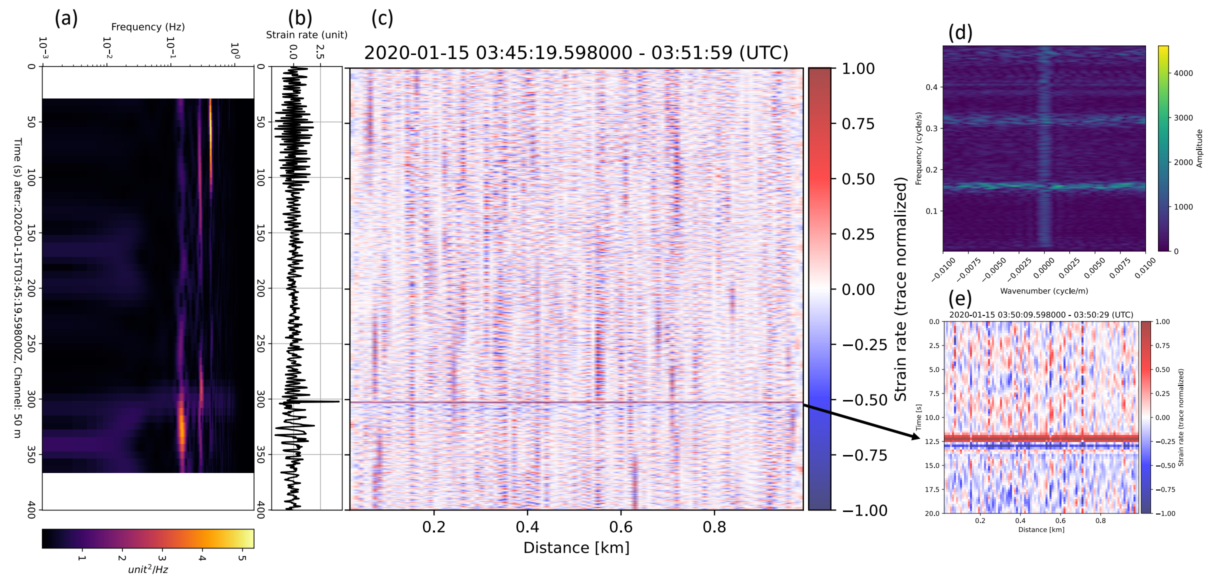

**Figure S2. (c) a 400-second example of noises between 0.01 to 1 Hz. (a) spectrogram of the channel at distance of 50 m. Time series is plotted in panel (b). (d) f-k transform of (c). (e) zoom in of (c) as indicated by the arrow.**

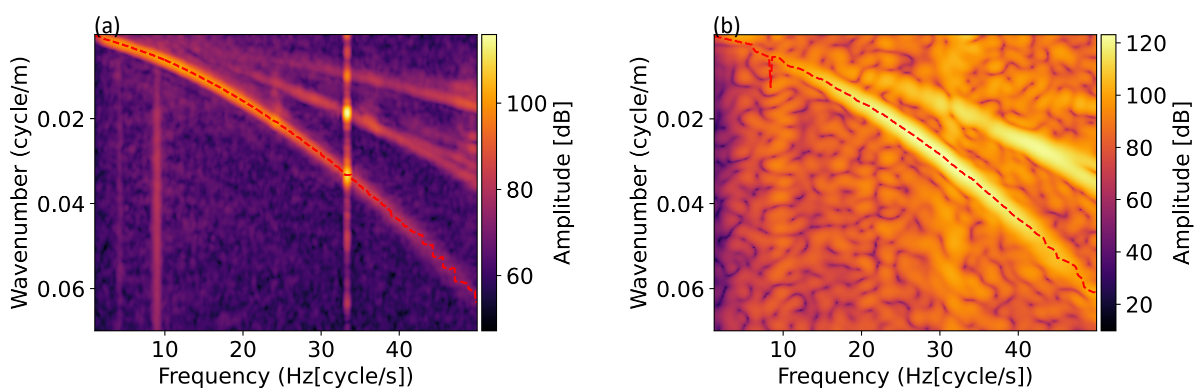

**Figure S3. Plots of f-k domain amplitude spectrum. (a) f-k for selective stacked cross-correlations (CCs), with picks of fundamental mode surface wave shown by a dashed line. (b) The same as (a) but for one active shot gather.**

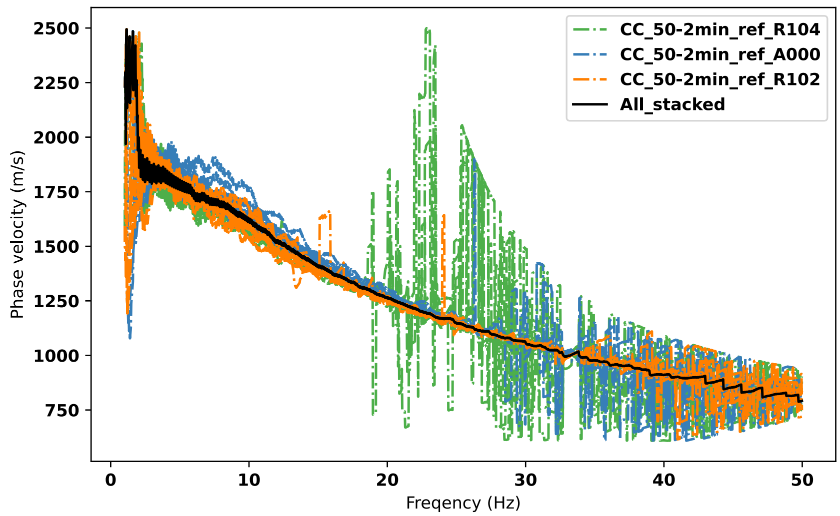


**Figure S4. Variation of dispersions from all 50-2min-CC stacks, compared with the stack over all selected 2-min CCs.**

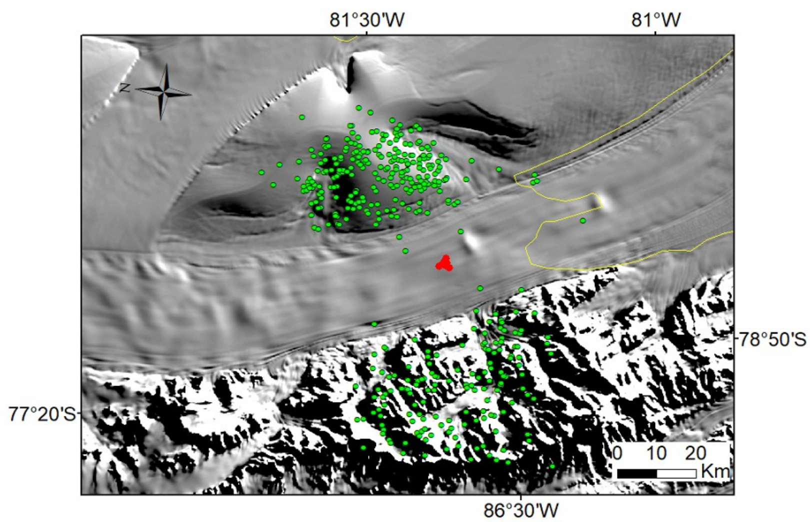


**Figure S5. Localized surface wave events using the geophone array, using travel time difference obtained from waveform cross-correlation.**